# Transient Natural Convection in Enclosures With Application to Solar Thermal Storage Tanks

D. T. Reindl

W. A. Beckman

J. W. Mitchell

Solar Energy Laboratory,
University of Wisconsin,
Madison, WI 53706

*Many previously studied natural convection enclosure problems in the literature have the bounding walls of the enclosure responsible for driving the flow. A number of relevant applications contain sources within the enclosure which drive the fluid flow and heat transfer. The motivation for this work is found in solar thermal storage tanks with immersed coil heat exchangers. The heat exchangers provide a means to charge and discharge the thermal energy in the tank. The enclosure is cylindrical and well insulated. Initially the interior fluid is isothermal and quiescent. At time zero, a step change in the source temperature begins to influence the flow. The final condition is a quiescent isothermal fluid field at the source temperature. The governing time-dependent Navier-Stokes and energy equations for this configuration are solved by a finite element method. Solutions are obtained for* $10^3 \leq Ra_D \leq 10^6$. *Scale analysis is used to obtain time duration estimates of three distinct heat transfer regimes. The transient heat transfer during these regimes are compared with limiting cases. Correlations are presented for the three regimes.*

## 1 Introduction

A crucial element in an active thermal solar energy system is storage. Since loads on a system typically do not directly coincide with the resource availability, a means to store collected energy for later use is essential. Many techniques and configurations have been devised to store thermal energy but detailed analyses of the techniques are limited. Two common sensible storage techniques are direct contact and indirect contact. In the direct contact case, a storage tank is charged and discharged by hot and cold fluid streams flowing directly in and out of the storage volume. Indirect contact storage strategies utilize one or more heat exchangers immersed in the storage volume to charge and discharge energy from the tank.

Several studies in the literature (Lavan and Thompson, 1977; Young and Baughn, 1981; Chan, Smereka, and Giusti, 1983; Guo, 1985; Lightstone, Raithby, and Hollands, 1989) have focused on analyzing direct contact thermal storage tanks while the studies for indirect contact storage tanks are scarce. Feiereisen et al. (1983) performed experiments using three different types of immersed heat exchangers: horizontal smooth-tube multipass, horizontal finned-tube spiraled, and a horizontal smooth-tube single-pass. The experiments yielded heat transfer relationships in the form of Nusselt number as a function of Rayleigh number for each heat exchanger configuration. The Nusselt and Rayleigh numbers were defined based on a log-mean temperature difference between the heat exchanger and tank temperature. Since this definition is not possible in the current investigation, the present results can not be compared with Feiereisen. From the experimental observations, Feiereisen et al. draw general conclusions regarding techniques to maximize the effectiveness of the immersed heat exchanger. Farrington built on the work of Feiereisen by performing experiments to determine overall loss coefficients and heat transfer performance from immersed coils in two commerical thermal storage tanks (Farrington, 1986) as well as four other heat exchanger configurations (Farrington and Bingham, 1986). Again, general conclusions are drawn regarding observed performance of the tanks and the immersed coil heat exchangers. These studies do not permit detailed investigation of the transient fluid flow and heat transfer processes within the enclosures.

The objective of this work is to gain insight into the fundamental physics of the fluid flow and heat transfer from an immersed coil heat exchanger in an enclosure and identify relevant parameters to correlate the transient heat transfer results. To accomplish these objectives, the governing transient Navier-Stokes and energy equations are solved by a finite element method. Solutions are obtained over a range of Rayleigh numbers ($10^3 \leq Ra_D \leq 10^6$) for a fixed enclosure size and exchanger location. This range is selected to include behavior from a conclusion dominated problem ($Ra_D = 10^3$) to the higher end of the laminar regime ($Ra_D = 10^6$).

## 2 Problem Definition

The problem configuration is an insulated cylindrical enclosure with a single loop coiled tube source as shown in Fig. 1.

The fluid filled enclosure is initially quiescent at a uniform

Contributed by the Solar Energy Division of THE AMERICAN SOCIETY OF MECHANICAL ENGINEERS for publication in the ASME JOURNAL OF SOLAR ENERGY ENGINEERING.

Manuscript received by the ASME Solar Energy Division, Dec. 15, 1991; final revision, Apr. 20, 1992. Associate Technical Editor: M. Wilden.

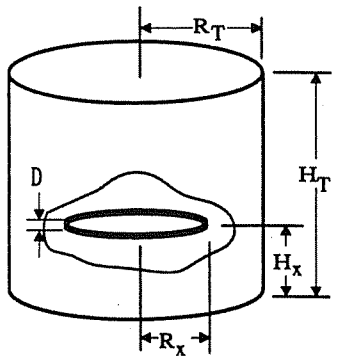


Fig. 1 Single coil tube in cylindrical enclosure configuration

temperature $T_o$. At time zero, a step change occurs in the wall temperature of the immersed heat exchanger to $T_w$. The final state is a quiescent flow field at a temperature equal to the heat exchanger coil temperature. These boundary conditions permit axisymmetric assumptions which greatly reduce the computations necessary to solve the problem.

The tank radius $R_T$ is half the tank height $H_T$ (a unit aspect ratio enclosure). The tank height is six times larger than the exchanger tube diameter $D$ and is twice the coil diameter. The heat exchanger is elevated to a position $H_x$ equal to 0.3 $H_T$ and has a radius $R_x$ equal to 0.25 $H_T$. Thus, the complete geometric problem is scaled based on the magnitude of the Rayleigh number. The primary quantity of interest is the average heat flux from the exchanger (average Nusselt number based on the *initial* temperature difference). The working fluid (water) has constant properties with Pr = 5.42.

## 3 Mathematical Formulation and Solution Technique

Assuming that the immersed heat exchanger is isothermal, the problem reduces from three-dimensional to two-dimensional axisymmetric. (In reality, the flow is three-dimensional because of azimuthal variation in temperature as the fluid moves through the interior of the heat exchanger from inlet to outlet.) The governing differential equations for this configuration can be nondimensionalized using the variables shown in Table 1.

Table 1 Cylindrical coordinate variable nondimensionalization

| | |
|---|---|
| $r^* = r/D$ | $z^* = z/D$ |
| $v_r^* = v_r/U$ | $v_z^* = v_z/U$ |
| $T^* = (T - T_o)/(T_w - T_o)$ | $P^* = P/\rho U^2$ |
| $t^* = tU/D$ | $U = \sqrt{g\beta(T_w - T_o)D}$ |

After dropping the * superscripts, the governing dimensionless differential equations for this configuration are

**Conservation of Mass:**

$$\frac{1}{r}\frac{\partial}{\partial r}(rv_r) + \frac{\partial}{\partial z}(v_z) = 0. \tag{1}$$

**Radial Momentum:**

$$\frac{\partial v_r}{\partial t} + v_r\frac{\partial v_r}{\partial t} + v_z\frac{\partial v_r}{\partial z} = -\frac{\partial P}{\partial r} + \sqrt{\frac{\mathrm{Pr}}{\mathrm{Ra}_D}}\left[\frac{1}{r}\frac{\partial}{\partial r}\left(r\frac{\partial v_r}{\partial r}\right) + \frac{\partial^2 v_r}{\partial z^2} - \frac{v_r}{r^2}\right]. \tag{2}$$

**Axial Momentum:**

$$\frac{\partial v_z}{\partial t} + v_r\frac{\partial v_z}{\partial r} + v_z\frac{\partial v_z}{\partial z} = -\frac{\partial P}{\partial z} + \sqrt{\frac{\mathrm{Pr}}{\mathrm{Ra}_D}}\left[\frac{1}{r}\frac{\partial}{\partial r}\left(r\frac{\partial v_z}{\partial r}\right) + \frac{\partial^2 v_z}{\partial z^2}\right] + T. \tag{3}$$

**Energy:**

$$\frac{\partial T}{\partial t} + v_r\frac{\partial T}{\partial r} + v_z\frac{\partial T}{\partial z} = \frac{1}{\sqrt{\mathrm{Ra}_D\mathrm{Pr}}}\cdot\left[\frac{1}{r}\frac{\partial}{\partial r}\left(r\frac{\partial T}{\partial r}\right) + \frac{\partial^2 T}{\partial z^2}\right]. \tag{4}$$

## Nomenclature

$A$ = area of computational domain
$D$ = heat exchanger tube diameter (m)
$g$ = acceleration due to gravity ($m^2/s$)
$H_T$ = cylindrical enclosure height (m)
$H_x$ = tube heat exchanger height (m)
$k$ = thermal conductivity (W/m-°C)
$L$ = characteristic length (m)
$n$ = normal directed vector
$\overline{\mathrm{Nu}}$ = average Nusselt number based on $D$ and $(T_w - T_o)$
$P$ = pressure ($N/m^2$)
Pr = Prandtl number ($\nu/\alpha$)
$q$ = heat flux ($W/m^2$)
$Q$ = flow rate ($m^3/s$)
$r$ = radial coordinate distance (m)
$r_x$ = tube heat exchanger radius (m)
$\mathrm{Ra}_D$ = Rayleigh number based on tube diameter ($g\beta D^3\Delta T/\nu\alpha$)
$R_T$ = cylindrical enclosure radius (m)
$r_x$ = heat exchanger tube radius (m)
$R_X$ = heat exchanger coil radius (m)
$t$ = time (s)
$T_o$ = initial temperature (°C)
$T_w$ = temperature of heat exchanger tube (°C)
$\overline{T}$ = bulk temperature, $\{\int T dA\}/A$
$U$ = characteristic velocity, $\sqrt{g\beta(T_w - T_o)D}$ (m/s)
$V$ = characteristic scale velocity, velocity vector
$v_r$ = radial component of velocity (m/s)
$v_z$ = axial component of velocity (m/s)
$z$ = axial coordinate distance (m)

**Greek symbols**

$\alpha$ = thermal diffusivity ($m^2/s$)
$\beta$ = volume expansion coefficient (1/K)
$\Delta T$ = initial temperature difference $(T_w - T_o)$ (°C)
$\Delta t_c$ = duration of conduction dominated regime (s)
$\Delta t_{qs}$ = duration of quasi-steady regime (s)
$\delta_T$ = characteristic thermal boundary layer thickness (m)
$\epsilon$ = penalty parameter, (1E − 8)
$\eta$ = relative tube exchanger height $(H_x/H_T)$
$\kappa$ = relative exchanger radial location $(R_x/H_T)$
$\nu$ = kinematic viscosity ($m^2/s$)
$\rho$ = density ($kg/m^3$)
$\phi$ = relative tube radius $(r_x/H_T)$
$\theta$ = angular coordinate around heat exchanger tube

**Superscripts**

* = dimensionless quantity
− = bulk average quantity

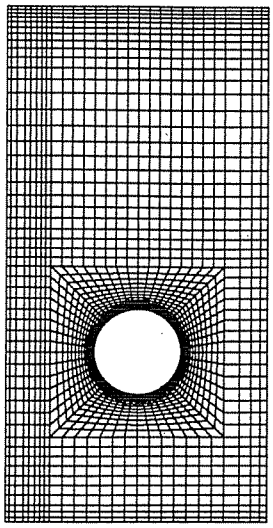

Fig. 2 Mesh for cylindrical cavity, 2128 quadratic elements

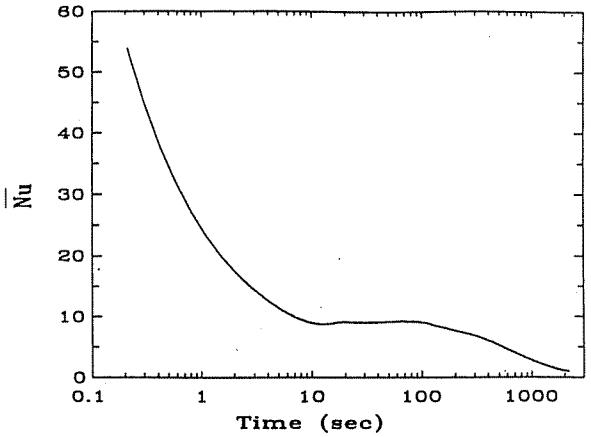


Fig. 3 Transient heat transfer response for $Ra_D = 10^5$

The elements are nine-node quadrilaterals with quadratic bases for both the velocity and temperature components. Element integrals are performed numerically by a third-order Gaussian quadrature. The finite element approximation reduces the system of partial differential equations to a system of ordinary differential equations. Time integration of the system ordinary differential equations is accomplished by an adaptive second-order implicit trapezoid rule.

**Boundary Conditions:**

| | | | |
|---|---|---|---|
| @ $r=0$ | $0 \le z \le H_T/D$ | $v_r=0,\ \partial v_z/\partial r=0$ | $\partial T/\partial n=0$ |
| @ $r=R_T/D$ | $0 \le z \le H_T/D$ | $v_r=v_z=0$ | $\partial T/\partial n=0$ |
| @ $z=0$ | $0 \le r \le R_T/D$ | $v_r=v_z=0$ | $\partial T/\partial n=0$ |
| @ $z=H_T/D$ | $0 \le r \le R_T/D$ | $v_r=v_z=0$ | $\partial T/\partial n=0$ |
| @ cylinder surface | | $v_r=v_z=0$ | $T=1.$ |

**Initial Conditions:**

for all $r$ for all $z$ $v_r=v_z=0$ $T=0.$

A quantity of primary interest in this study is the average Nusselt number (average dimensionless heat flux) $\overline{\mathrm{Nu}}$ over the tube. The average Nusselt number is the integral of the local flux over the arc length of the heat exchanger boundary as given by

$$\overline{\mathrm{Nu}} = \int_0^{2\pi} \left.\frac{\partial T}{\partial n}\right|_w d\theta \tag{5}$$

where $\theta$ is the angular coordinate around the tube. Note that the above definition of the average Nusselt number is based on the initial temperature difference $(T_w - T_o)$ and not the more traditional temperature difference $(T_w - \overline{T})$ where $\overline{T}$ is the bulk temperature in the enclosure.

The governing partial differential equations given by Eqs. (1)–(4) are solved in a primitive variable form with FIDAP (n.d.) using a Galerkin finite element approximation. A penalty function approach is used to approximate pressure in the primitive variable formulation. The penalty method relaxes the strict continuity requirement by letting

$$\frac{1}{r}\frac{\partial}{\partial r}(r v_r) + \frac{\partial}{\partial z}(v_z) = -\epsilon P \tag{6}$$

where $\epsilon$ is a penalty parameter ($\epsilon \sim 10^{-5} - 10^{-9}$). Solving Eq. (6) for pressure and substituting the result into Eqs. (2) and (3) eliminates pressure from the system of differential equations. The pressure can be obtained subsequently by post-processing using $P = -[\partial(r v_r)/r\partial r + \partial v_z/\partial z]/\epsilon$. The most obvious advantage of the penalty method is a reduction in the degrees-of-freedom for the particular system being solved; however, care must be exercised in selection of elements used and the value of the penalty parameter. Based on previous work (Marshall, Heinrich, Zienkiewicz, 1978; Reddy and Satake, 1980), the penalty parameter for the present computations is fixed at $\epsilon = 10^{-8}$. For a further discussion of the penalty method, see Hughes, Liu, and Brooks (1979) and Sani, Gresho, Lee, and Griffins (1981).

As a preface to this work, the differentially heated square cavity problem was solved with FIDAP. A graded mesh of $30 \times 30$ elements yielded excellent agreement with the de Vahl Davis benchmark solution (de Vahl Davis and Jones, 1983) (e.g., $\overline{\mathrm{Nu}}$ results were within 0.33 percent of de Vahl Davis over the range of Ra). Although the current geometry and conditions differ considerably from the differentially heated cavity, agreement with the de Vahl Davis benchmark lends some confidence in the ability of the code to model strongly coupled flows.

## 4 Results

This section presents results for the cylindrical enclosure computations. A significant effort has been made to assure the final solutions are independent of the spatial and temporal computational meshes. The mesh refinement techniques used here are identical to those given by Reindl et al. (1991). The spatial mesh employed in the present computations is shown in Fig. 2.

All computations are carried out on a Cray Y-MP8/864 computer. Referring to the mesh in Fig. 2, the CPU time required to obtain transient results depends on the magnitude of the Rayleigh number. Typical run times ranged from three hours ($Ra = 10^3$) to 20 hours ($Ra = 10^6$). Computations at higher Rayleigh numbers were not attempted due to computational resource limits.

A typical response for the heat transfer from the immersed coil is shown in Fig. 3.

Since very little fluid motion exists in the early transient, the heat transfer from the coil is dominated by pure conduction. The conduction heat transfer establishes a thermal boundary layer in the neighborhood of the heat exchanger which grows with time. The heat flux reaches a local minimum and subsequently begins to increase before reaching a nearly constant value that is maintained during a quasi-steady period.

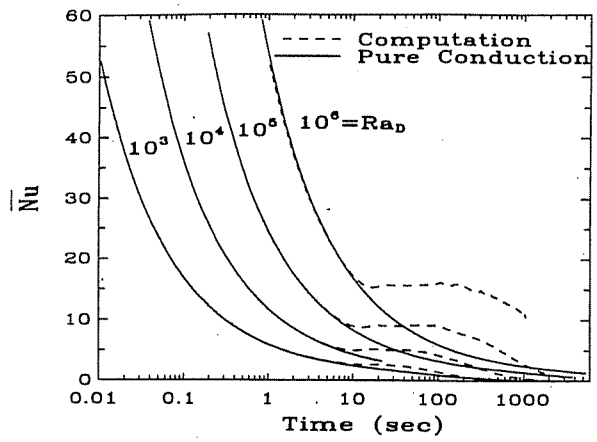


Fig. 4 Transient heat transfer results including pure conduction solutions for $10^3 \le Ra_D \le 10^6$

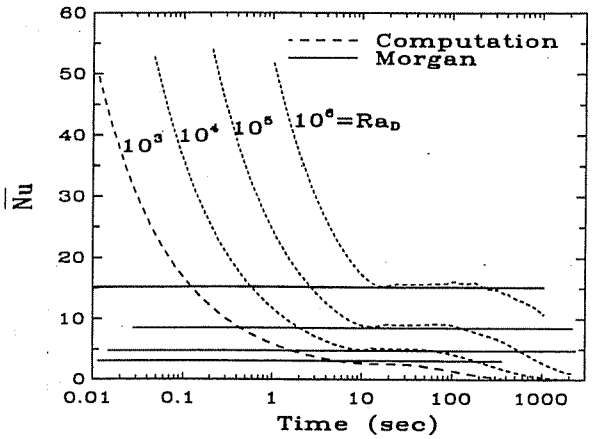


Fig. 5 Transient heat transfer results including Morgan correlation for the respective Rayleigh number $10^3 \le Ra_D \le 10^6$

The local minimum in heat flux corresponds to a local maximum in the thermal boundary layer thickness which quickly decreases as significant fluid motion near the tube begins, marking the end of the conduction dominated heat transfer regime. As the fluid motion develops, the heat flux increases slightly to its quasi-steady value. During the quasi-steady period, thermal and momentum boundary layers are fully established and the heat exchanger behaves as if it were immersed in an infinite medium. As the transient progresses, the heat flux decreases due to the increase in enclosure bulk fluid temperature. Thus, the transient heat transfer response in characterized by three distinct regimes: pure conduction, quasi-steady, and decay periods.

**4.1 Limiting Cases.** The mesh refinement techniques were performed (as described in Reindl et al. (1991)) in an attempt to determine spatial and temporal mesh densities which yield accurate solutions. There are two additional comparisons that can be made to lend confidence in the current solutions. The heat transfer results can be compared with two limiting cases: pure conduction and natural convection from a horizontal cylinder in an infinite medium.

Figure 4 shows the pure conduction and actual computed solutions for the complete range of Rayleigh numbers.

It is clear that the early transient is conduction dominated. Also, at low Rayleigh numbers ($Ra_D \le 10^3$), the heat transfer is largely conduction dominated throughout the entire transient.

The nearest analogy to compare the heat transfer during the quasi-steady regime is the long horizontal cylinder in an infinite medium. Unfortunately, Morgan (1975) reveals a wide disparity in the reported values of the average Nusselt number as a function of Rayleigh number for the horizontal cylinder in an infinite medium. The computed results over the quasi-steady regime are compared with a proposed correlation given by Morgan (evaluated at the respective Rayleigh numbers) in Fig. 5. Another source for comparing the current results is based on a correlation by Churchill and Chu (1975). The results from Churchill and Chu, Morgan, and the computed average Nusselt number over the quasi-steady period are summarized in Table 2 for each order of Rayleigh number.

Table 2 Average Nusselt number results of current computations ($\overline{Nu}$) compared with corrections from Morgan ($\overline{Nu}_{Morgan}$) and Churchill and Chu ($\overline{Nu}_{C\&C}$)

| $Ra_D$ | $\overline{Nu}$ | $\overline{Nu}_{Morgan}$ | $\overline{Nu}_{C\&C}$ |
|---|---|---|---|
| $10^3$ | 2.96 | 3.11 | 3.02 |
| $10^4$ | 5.14 | 4.80 | 5.15 |
| $10^5$ | 9.08 | 8.54 | 9.31 |
| $10^6$ | 15.67 | 15.20 | 17.62 |

The present computations compare well with Churchill and Chu at Rayleigh numbers up to $10^5$ and with Morgan at $10^6$. Considering the variation in the previously published results reported by Morgan, the current quasi-steady results compare reasonably well with either Churchill and Chu or Morgan.

The limiting cases of pure conduction and infinite medium provides an independent basis for comparing the behavior and accuracy of the current results during the first two regimes. The behavior of the fluid flow and heat transfer during the decay period is rather complex as the bulk temperature in the enclosure begins to rise and fluid velocities diminish. There are no simple limiting cases to represent the heat transfer during the decay period.

**4.2 Scale Analysis.** Temporal behavior of the pure conduction and quasi-steady regimes are well characterized by the limiting cases shown in Figs. 4–5. It is useful to predict the time duration of the conduction and quasi-steady regimes as well as determine the appropriate parameters to correlate the decay period. This can be accomplished by the use of scaling analysis. Scale analysis is a technique which considers the governing differential equations only in an order-of-magnitude sense. Patterson and Imberger (1980) used scaling analysis extensively in their study of a differentially heated square and their work is used as a basis for the estimates derived here. Interestingly, the scale estimates developed for the geometry considered here are similar to those which arise for the differentially heated cavity.

The following sequence of estimates attempts to predict the time duration of the conduction dominated regime. Considering the dimensional form of the energy equation in an order of magnitude sense, e.g.,

$$\frac{\partial T}{\partial t}+\nu_r\frac{\partial T}{\partial r}+\nu_z\frac{\partial T}{\partial z}\alpha\left\{\frac{1}{r}\frac{\partial}{\partial r}\left(r\frac{\partial T}{\partial r}\right)+\frac{\partial^2 T}{\partial z^2}\right\}$$

$$\Rightarrow \frac{\Delta T}{\Delta t},\ \nu_r\frac{\Delta T}{\delta_T},\ \nu_z\frac{\Delta T}{D}\sim\frac{\alpha}{r}\frac{\Delta T}{\delta_T},\ \alpha\frac{\Delta T}{\delta_T^2},\ \alpha\frac{\Delta T}{D^2}$$

where $\Delta T=(T_w-T_o)$, $\Delta t$ is the time duration, $\delta_T$ is a characteristic thermal boundary layer thickness, and $D$ is the heat exchanger tube diameter. Assuming the velocity components are small during the early transient and the boundary layer thickness is much smaller than the tube diameter ($\delta_T \ll D$), the remaining terms balance providing an estimate for the thermal boundary layer thickness.

$$\delta_T \sim (\alpha \Delta t)^{1/2} \tag{7}$$

Considering the dimensional form of axial momentum (Eq. (3)), the buoyancy force $g\beta\Delta T$ accelerates fluid within the

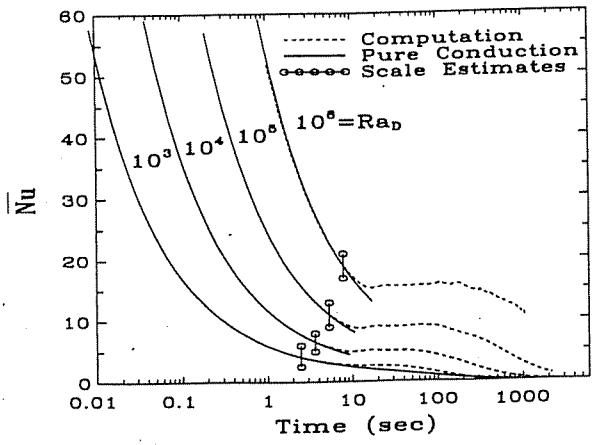


Fig. 6 Scale estimates for the end of the conduction dominated regime

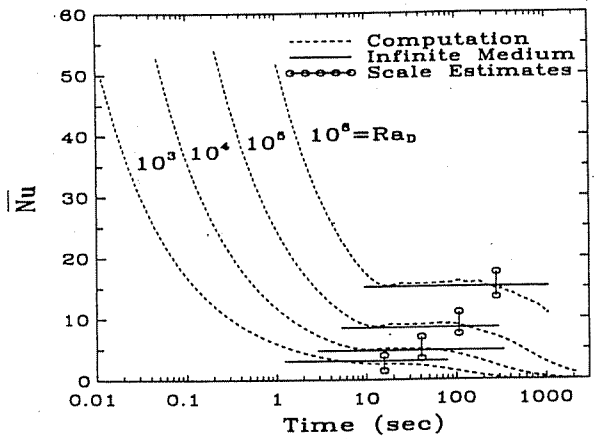


Fig. 7 Scale estimates for the end of the quasi-steady regime

boundary layer $\delta_T$ and for a Prandtl number greater than unity, the viscous force terms $\nu v_z/\delta_T^2$ dominates the inertia force $v_z/\Delta t$ term. The resulting balance between the buoyancy and viscous force terms yields an estimate of the vertical velocity component.

$$v_z \sim \frac{g\beta\Delta T}{\mathrm{Pr}}\Delta t \tag{8}$$

An energy balance on the thermal boundary layer imposes a balance between the conducted energy from the heat exchanger and that convected away.

$$v_z\frac{\Delta T}{D} \sim \alpha\frac{\Delta T}{\delta_T^2}$$

The above expression can be simplified by Eqs. (7) and (8) which results in an estimate for the time duration of the conduction dominated regime. Conduction limit time estimates from Eq. (9) are shown in Fig. 6. The scale estimates accurately predict the duration of the conduction dominated regime.

$$\Delta t_c \sim \frac{D^2}{\Delta \mathrm{Ra}_D^{1/2}} \tag{9}$$

At the end of the conduction dominated regime, $v_z$ becomes

$$v_z \sim \frac{\mathrm{Ra}_D^{1/2}\alpha}{D}$$

and the boundary layer thickness is $\delta_T \sim D/\mathrm{Ra}_D^{1/4}$. Assuming the volume flow of fluid through the boundary layer is constant during the quasi-steady period, the flow rate $\dot{Q}$ is given by

$$\dot{Q} \sim v_z\delta_T \sim \alpha \mathrm{Ra}_D^{1/4}.$$

The end of the quasi-steady regime occurs when the temperature in the tank begins to rise significantly. This will surely occur if a volume of fluid equivalent to that above the heat exchanger is circulated through the coil thermal boundary layer. The time required to circulate the volume of fluid above the heat exchanger through the thermal boundary layer around the heated coil yields the quasi-steady period duration estimate.

$$\Delta t_{qs} \sim \frac{r_x^2\gamma[1-(\eta+\phi)]}{2\alpha\phi^2\,\mathrm{Ra}_D^{1/4}} \tag{10}$$

where $r_x = D/2$, $\gamma = R_T/H_T$, $\eta = H_x/H_T$, and $\phi = r_x/H_T$. The quasi-steady time duration scale estimates shown in Fig. 7 agree well with the apparent end of the quasi-steady period identified by the onset of the computed heat transfer diverging from the infinite medium case.

The above scale estimates can be used to approximate the time duration of the conduction and quasi-steady regimes whose temporal behavior are well characterized by the limiting cases given in Section 4.1. It is desirable to identify relevant parameters to correlate the decay period; scale analysis is used to identify these parameters.

An energy balance on the heat exchanger yields a result which requires that the conducted energy must balance the convected energy.

$$k\frac{(T_w-\overline{T})}{\delta_T} \sim \frac{\overline{\mathrm{Nu}}k}{D}(T_w-T_o). \tag{11}$$

Since $\delta_T$ is not constant as the decay period progresses, the expression for the characteristic thermal boundary thickness must be modified.

$$\delta_T \sim \frac{D}{\mathrm{Ra}_D^{1/4}} \rightarrow \bar{\delta}_T \sim \frac{D}{\overline{\mathrm{Ra}}_D^{1/4}}$$

where $\overline{\mathrm{Ra}}_D^{1/4}$ is the Rayleigh number based on the temperature difference $(T_w-\overline{T})$ similar to that used by Hall et al. (1988). Substituting the above expression in Eq. (11) results in an estimate for the Nusselt number.

$$\overline{\mathrm{Nu}} \sim (1-\overline{T}^*)^{5/4}\mathrm{Ra}_D^{1/4} \tag{12}$$

with $\overline{T}^* \equiv (\overline{T}-T_o)/(T_w-T_o)$ which is proportional to the fraction $f$ of the cavity heated to temperature $T_w$. Equation (12) is not a useful expression for correlating the Nusselt number since the bulk cavity temperature or heated fraction $f$ are required. An expression for the heated fraction can be found by considering an overall energy balance on the enclosure for the differentially heated fraction as

$$df = \frac{q\,dt}{mc(T_w-T_o)}. \tag{13}$$

Solving the above differential equation and applying the condition $@t=0, f=1$ gives an expression for the heated fraction which can be substituted into Eq. (12). The result is an expression to correlate the decay period heat transfer.

$$\overline{\mathrm{Nu}} = 0.5686\left[1+\frac{\alpha\kappa\phi^2\mathrm{Ra}_D^{1/4}t}{\gamma^2D^2}\right]^{-5}\mathrm{Ra}_D^{1/4} \tag{14}$$

where $\alpha$ is the thermal diffusivity, $\kappa = R_x/H_T$, $\phi = r_x/H_T$, $\gamma = R_T/H_T$, and $\mathrm{Ra}_D$ is defined based on the initial temperature difference. The coefficient 0.5686 is determined from a least squares fit of the decay period results for all orders of Rayleigh number. The correlation given by Eq. (14) explains 99.86 percent of the variation in the average Nusselt number over the decay period. The agreement between the correlated decay periods and the actual computed decay periods is demonstrated in Fig. 8 for $\mathrm{Ra}_D = 10^5$. Plots for other orders of Rayleigh number are similar.

For thermal storage, an important consideration is the time required to charge the tank or the transient bulk temperature response. Figure 9 shows the typical response of the bulk temperature in the enclosure.

It is clear that the majority of energy transfer into the tank occurs during the decay period.

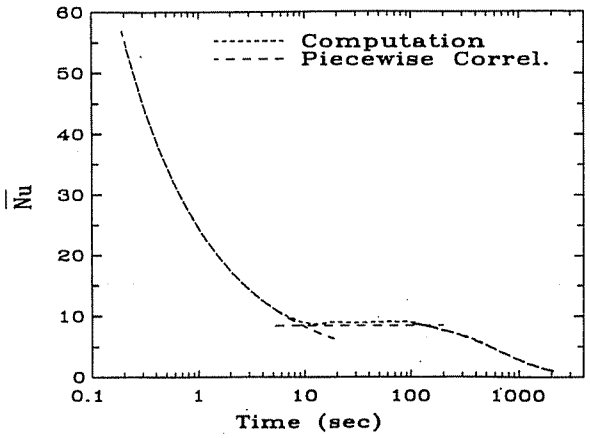


Fig. 8 Computed heat transfer response and piecewise heat transfer response composed of pure conduction, infinite medium, and the correlated decay period for $Ra_D = 10^5$

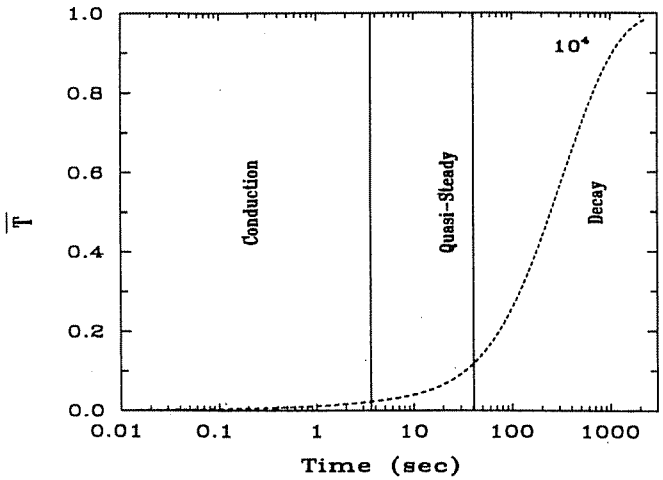


Fig. 9 Transient bulk temperature response that occurs during the respective regimes for $Ra_D = 10^4$

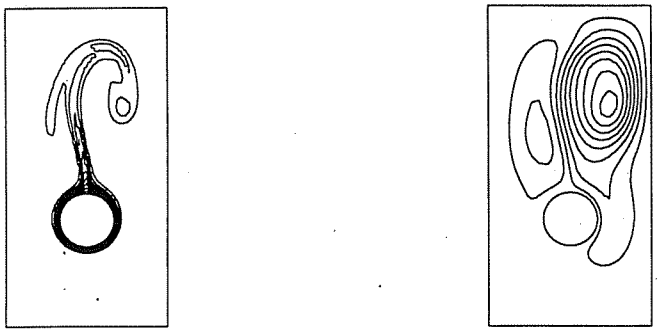


Fig. 10 Contour maps at $T^* = 61$ ($t = 140$ s), $Ra_D = 10^5$: (*a*) Isotherms, $T_{min} = 0.1$, $\Delta T = 0.1$, $T_{max} = 1.0$, i.e., 0.1(0.1)1.0; (*b*) Stream function, $\psi_{min} = 3.391$, $\Delta\psi = 0.452$, $\psi_{max} = 0.673$, i.e., −3.391(0.452)0.673

**4.3 Flow Field Results.** The transient evolution of the temperature and fluid flow fields in the present geometry are very complex. Farrington and Bingham (1986) used dye injection techniques and noted the complex behavior of the flow fields from the various heat exchanger configurations. In the case of a smooth coil heat exchanger, the authors noted unstable and swirling convection currents. Similar behavior is observed in this study.

This section presents results of the temperature and velocity flow fields for the case of $Ra_D = 10^5$. Figures 10(*a*) and 10(*b*)

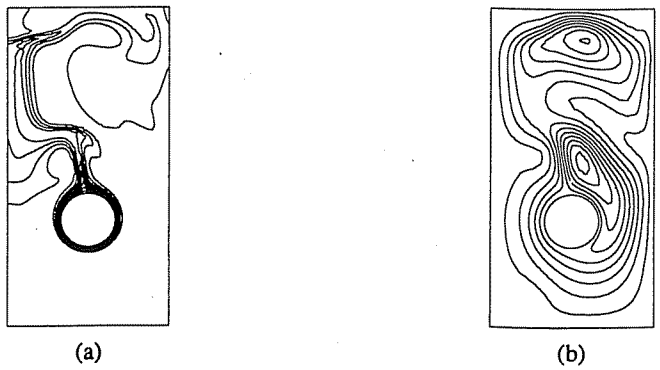


Fig. 11 Contour maps at $t^* = 101$ ($t = 232$ s), $Ra_D = 10^5$: (*a*) Isotherms, 0.1(0.1)1.0; (*b*) Stream function, −1.88(0.20)−0.07735

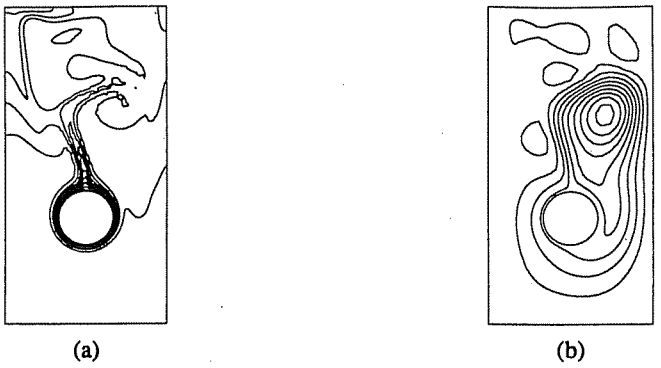


Fig. 12 Contour maps at $t = 141^*$ ($t = 323$), $Ra_D = 10^5$: (*a*) Isotherms, 0.1(0.1)1.0; (*b*) Stream function, −2.554(0.304)0.0955

show temperature and stream function[1] contours, respectively, at the time corresponding to the early quasi-steady period.

By this time in the quasi-steady regime, the velocity flow field near the cylinder is fully developed and the thermal plume above the cylinder is reaching the top of the enclosure. Two vortices circulate in opposite directions on either side of the cylinder with a large component of flow proceeding down the center of the enclosure.

Figure 11 shows the results at a later time in the quasi-steady period. At this time, clockwise rotating eddies have formed above the cylinder and the core flow near the cylinder source in the center of the enclosure has reversed. The core of the enclosure above the cylinder is relatively warmer than fluid near the enclosure walls and stratification is not being induced.

The flow and temperature fields at a time corresponding to the end of the quasi-steady regime are shown below in Fig. 12. The end of the quasi-steady period is caused by the weakly stratified temperature field moving warmer fluid down near the cylinder source; thereby, reducing the temperature difference across the source. Core flow near the cylinder source has resumed its upward flow direction and several clockwise and counterclockwise eddies have formed.

Temperature and flow field results at a time well into the decay period are presented in Fig. 13. At this instant in the transient, the enclosure is 56 percent charged. The level of stratification is greater than that observed at the end of the quasi-steady period while the behavior of the flow field is quite different. As the driving force for flow decreases, the fluid does not have enough momentum to penetrate below the heat exchanger into the base of the enclosure. Only a small portion

[1] The stream function $\psi$ is defined by $u = \partial\psi/\partial y$, $v = -\partial\psi/\partial x$. This definition allows the generation of a contour which is everywhere tangent to the local velocity vector. The change in stream function is an exact differential given by $\Delta\psi = \int(V \cdot n)d\Gamma$ where $V$ is the velocity and $\gamma$ is a general path of integration.

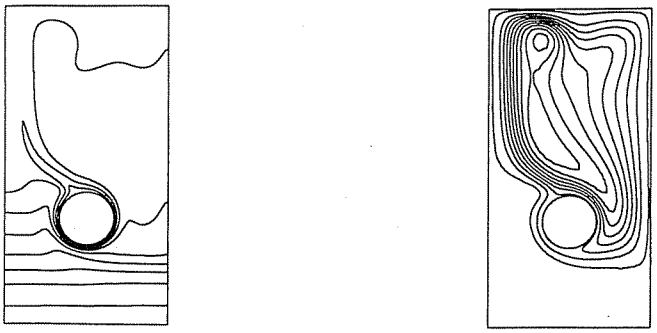


Fig. 13 Contour maps at $t^* = 373$ ($t = 855$ s), $Ra_D = 10^5$: (*a*) Isotherms, 0.1(0.1)1.0; (*b*) Stream function, $-0.6326(0.06917) - 0.01008$

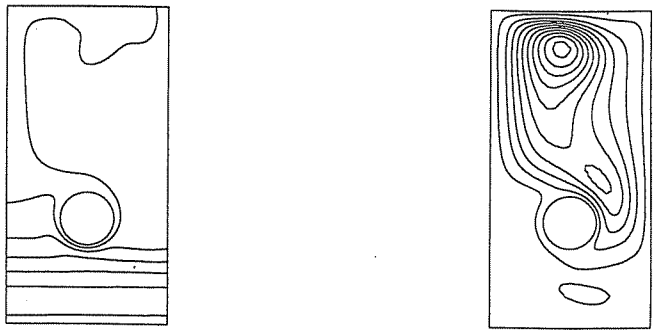


Fig. 14 Contour maps at $t^* = 868$ ($t = 1991$ s), $Ra_D = 10^5$: (*a*) Isotherms, 0.4(0.1)1.0; (*b*) Stream function, $0.6394(0.068866) - 0.02146$

of fluid below the heat exchanger is entrained in the boundary layer and heated. The fluid motion is largely confined to a clockwise rotating vortex in the upper portion of the enclosure.

The temperature and flow fields in Fig. 14 correspond to the late decay period when the enclosure is 80 percent charged. Note the similarity in temperature and flow field results in Fig. 14 with those of Fig. 13. The level of stratification is similar to that exhibited earlier in the decay period. The focus of the elongated clockwise rotating vortex has moved directly above the heat exchanger as the magnitude of the velocities continue to diminish.

## 5 Conclusions

A cylindrical enclosure with an immersed circular coil heat exchanger is considered. Computations are performed for a range of Rayleigh numbers and three distinct heat transfer regimes are identified. Initially, the transient heat transfer process is characterized by pure conduction. This is followed by a quasi-steady regime during which the heat transfer agrees with a horizontal cylinder immersed in an infinite medium. The final regime is a decay period. Scale analysis is used to determine time estimates for the duration of the regimes and identify the appropriate parameters to correlate the decay period heat transfer.

## Acknowledgments

This work has been supported by the Solar Applications for Buildings, Conservation and Renewable Energy Division, U.S. Department of Energy. Computational resources have been provided by the San Diego Supercomputer Center.

## References

Chan, A. M. C., Smereka, P. S., and Giusti, D., 1983, "A Numerical Study of Transient Mixed Convection Flows in a Thermal Storage Tank," ASME JOURNAL OF SOLAR ENERGY ENGINEERING, Vol. 105, pp. 246-253.

Churchill, S. W., and Chu, H. H. S., 1975, "Correlating Equations for Laminar and Turbulent Free Convection From a Horizontal Cylinder," *International Journal of Heat and Mass Transfer*, Vol. 18, p. 1049.

de Vahl Davis, G., and Jones, I. P., 1983, "A Comparison Exercise," *International Journal for Numerical Methods in Fluids*, Vol. 3, pp. 227-248.

Farrington, R. B., 1986, "Test Results of Immersed Coil Heat Exchangers and Liquid Storage Tanks Used in the Packaged Systems Program," SERI Report No. TR-254-2841, June.

Farrington, R. B., and Bingham, C. E., 1986, "Testing and Analysis of Immersed Heat Exchangers," SERI Report No. TR-253-2866, Aug.

Feiereisen, T. J., Klein, S. A., Duffie, J. A., and Beckman, W. A., 1983, "Heat Transfer From Immersed Coils," Paper No. 82-WA/SOL-18, presented at ASME Winter Annual Meeting, Phoenix, 1982.

FIDAP, (n.d.), A Fluid Dynamics Analysis Package by Fluid Dynamics International, Evanston, IL.

Guo, K. L., 1985, "Numerical Study of Flow and Temperature Stratifications in a Liquid Thermal Storage Tank," ASME JOURNAL OF SOLAR ENERGY ENGINEERING, Vol. 107, pp. 15-20.

Hall, J. D., Bejan, A., and Chaddock, J. B., 1988, "Transient Natural Convection in a Rectangular Enclosure with One Heated Side Wall," *International Journal of Heat and Fluid Flow*, Vol. 9, No. 4, pp. 396-404.

Hughes, T. J. R., Liu, W. K., and Brooks, A., 1979, "Finite Element Analysis of Incompressible Viscous Flows by the Penalty Function Formulation," *Journal of Computational Physics*, Vol. 30, pp. 1-60.

Lavan, Z., and Thompson, J., 1977, "Experimental Study of Thermally Stratified Hot Water Storage Tanks," *Solar Energy*, Vol. 19, pp. 519-524.

Lightstone, M. F., Raithby, G. D., and Hollands, K. G. T., 1989, "Numerical Simulation of the Charging of Liquid Storage Tanks: Comparison with Experiment," ASME JOURNAL OF SOLAR ENERGY ENGINEERING, pp. 225-231.

Marshall, R. S., Heinrich, J. C., and Zienkiewicz, O. C., 1978, "Natural Convection in a Square Enclosure by a Finite-Element, Penalty Function Method Using Primative Fluid Variables," *Numerical Heat Transfer*, Vol. 1, pp. 315-330.

Morgan, V. T., 1975, "The Overall Convective Heat Transfer From Smooth Circular Cylinders," *Advances in Heat Transfer*, Vol. 11, pp. 199-263.

Patterson, J., and Imberger, J., 1980, "Unsteady Natural Convection in a Rectangular Cavity," *Journal of Fluid Mechanics*, Vol. 100, pp. 65-86.

Reddy, J. N., and Satake, A., 1980, "A Comparison of a Penalty Finite Element Model with the Stream Function-Vorticity Model of Natural Convection in Enclosures," ASME JOURNAL OF SOLAR ENERGY ENGINEERING, Vol. 102, pp. 659-666.

Reindl, D. T., Beckman, W. A., Mitchell, J. W., and Rutland, C. W., 1991, "Benchmarking Transient Natural Convection in an Enclosure," 91-HT-8, presented at ASME-NHT, Minneapolis.

Sani, R. L., Gresho, P. M., Lee, R. L., and Griffins, D. F., 1981, "The Cause and Cure (?) of the Spurious Pressures Generated by Certain GFEM Solutions of the Navier-Stokes Equation," *International Journal of Numerical Methods in Fluids*, Vol. 3, pp. 227-248.

Young, M. E., and Braughn, J. W., 1981, "An Investigation of Thermal Stratification in Horizontal Storage Tanks," ASME JOURNAL OF SOLAR ENERGY ENGINEERING, Vol. 103, pp. 286-290.